Supporting Information

Heterogeneously Nd^{3+} Doped Single Nanoparticles for NIR-induced Heat Conversion, Luminescence, and Thermometry

Lukasz Marciniak[1], Aleksandra Pilch[1], Sebastian Arabasz[2], Dayong Jin[3], A. Bednarkiewicz[1]*

[1]Institute of Low Temperature and Structure Research, Polish Academy of Sciences, Okólna 2, 50-422 Wroclaw, Poland

[2] Wroclaw Research Centre EIT+, Stablowicka 147, Wroclaw, Poland

[3]Institute for Biomedical Materials and Devices (IBMD), Faculty of Science, University of Technology Sydney, NSW, 2007, Australia

* corresponding author: a.bednarkiewicz@int.pan.wroc.pl

KEYWORDS optical heating, optical thermometry, hybrid nanoparticles, smart core-shell

The following four monodispersed samples have been synthesized: $NaNdF_4$ (hereafter alternatively referred to as 100Nd), NaYF4@$NaYF_4$:1%Nd (Y@1Nd), $NaNdF_4$ @ $NaYF_4$:1%Nd (100Nd@1Nd) and $NaNdF_4$@ $NaYF_4$ @ 1%Nd^{3+} :$NaYF_4$ (100Nd@Y@1Nd), where '@' symbol indicates core @ shell composition following the traditional notation.

The crystal structures and the phase purity of $NaNdF_4$, $NaYF_4$ @ $NaYF_4$:1%Nd, $NaNdF_4$@$NaYF_4$:1%Nd and $NaNdF_4$@ $NaYF_4$@1%Nd^{3+}:$NaYF_4$ nanocrystals were examined by XRD, as it shown at Figure S1. The reflections in the XRD pattern of $NaNdF_4$ core only material belong to the hexagonal $NaNdF_4$ structure (according to reference ICSD#18005). The reflexes on the XRD patterns of the other samples shall be the mixture of both hexagonal $NaNdF_4$ and $NaYF_4$ structures, but the experimental reflections are resembling the ones of the hexagonal $NaYF_4$ structure (reference ICDD#04-011-3581). The lattice parameters obtained from Rietveld refinement of XRD pattern are listed in Table 1. The slight differences in the relative peak intensities can be assigned to the variations of the preferential orientation of the nanoparticles.

Hexagonal β-phase is controversial over the cation sites and distribution. Usually $NaNdF_4$ structure with space group P-6 and Z=1.5 is used as a model for the hexagonal form. It has three different cation sites, 9-fold coordinated Y^{3+} position, 9-fold coordinated mixed Na^+/Y^{3+} position and 6-fold coordinated site that may be occupied by Na^+ exclusively. Ionic radius of 9-fold coordinated Y3+ and Nd3+ are equal to 1.075 and 1.163 respectively ["Revised Effective Ionic Radii and Systematic Studies of Interatomic Distances in Halides and Chalcogenides" By R. D. Shannon. ActaCrystallographica. (1976). A32, Pages 751-767.]. Recently it was shown, however, that β-phase is better described in P63/m symmetry where Na^+ ions may locate in the centers of trigonally compressed octahedrons whereas Y^{3+} ions may occupy only one mixed Y^{3+}/Na^+ site with 9-fold coordination. The Y^{3+} sites are substituted randomly with other lanthanides ions.It is interesting to note, that he pattern of the core is clearly shifted to lower angles (reflection at ~17 and ~30 deg), in respect to the reference $NaNdF_4$ pattern, whereas an opposite trend is observed for the shell material ($NaYF_4$ @ $NaYF_4$:1%Nd) in respect to the $NaYF_4$ reference. The reason for such unexpected behaviour can originate from a few reasons. Firstly, the reference materials are dedicated to microcrystalline materials, which may differ from nano-sized powders. Secondly, different sample thickness, may also artificially shift the reflexes to lower or higher angles.

Distinguishing the $NaYF_4$ from $NaNdF_4$ is impossible and finding the two phases in the core-shell materials is very difficult, since both structures are isostructural and have the same XRD patters. For the NaNdF4 the 2θ ~30 deg two reflection shell be found, but they are so close they overlap with each other.

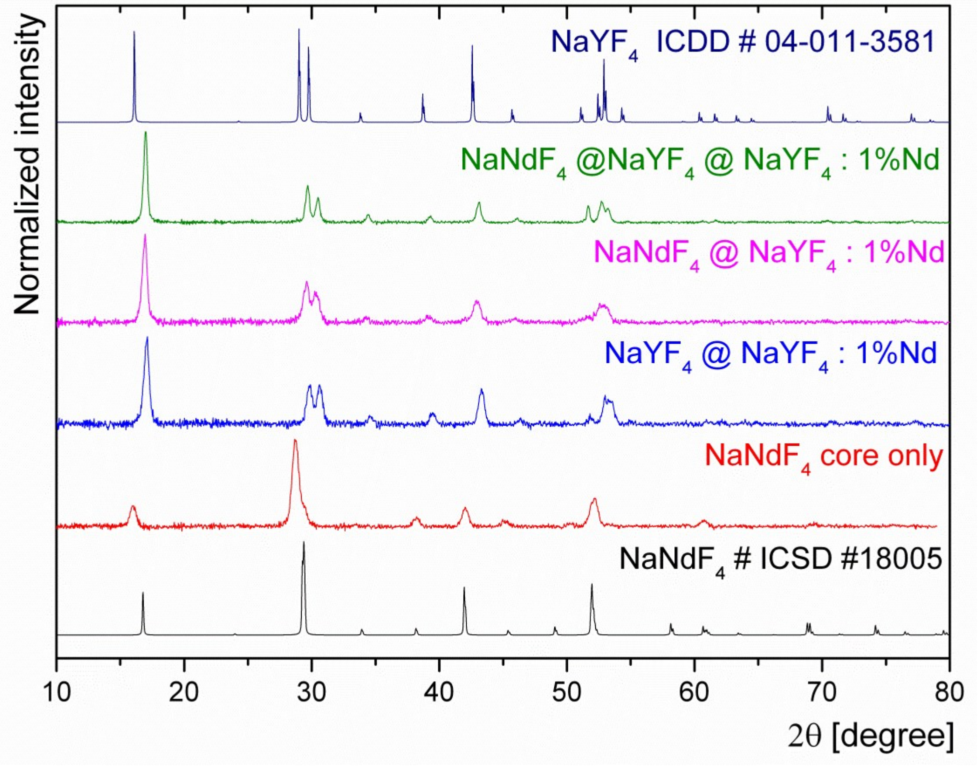

a = 5.95 Å
c = 3.53 Å
V = 108.23 Å^3

a = 6.0187(4) Å
c = 3.5404(8) Å
V = 111.07 Å^3

a = 6.0400(5) Å
c = 3.5534(9) Å
V = 112.27 Å^3

a = 5.9894(6) Å
c = 3.5240(8) Å
V = 109.48 Å^3

a = 6.0049(4) Å
c = 3.560(1) Å
V = 111.16 Å^3

a = 6.1090(7) Å
c = 3.7160(5) Å
V = 120.1 Å^3

Figure S1. XRD patterns of the synthesized nanocrystals versus $NaYF_4$ and $NaNdF_4$ standards.

Table 1. The average size (from the STEM-HAADF images) of synthesized nanoparticles. The average sizes of the Core, Core @ Shell and Core @ Shell @ Shell demonstrate the values obtained for NPs of successive steps of the synthesis.

Sample	**Core**		**Core @ Shell**		**Core @ Shell @ Shell**	
	Width	Length	Width	Length	Width	Length

	[nm]	[nm]	[nm]	[nm]	[nm]	[nm]
$NaNdF_4$ @ $NaYF_4$:1%Nd	17	30	23	32	-	-
$NaNdF_4$ @ $NaYF_4$ @ $NaYF_4$:1%Nd	24	44	28	51	32	61
$NaNdF_4$	17	30	-	-	-	-

Figure S2 shows the representative STEM-HAADF images and size distribution histograms of synthesized nanocrystals/particles. The images confirm acceptable homogeneity of the shapes of the nanocrystals. The average values in terms of width and length are included in Table 1. The core only nanocrystals are of average size 24x44 nm. As expected, with successive covering of their surface with subsequent shells, gradual increase of their volume is observed to 28x51 nm for 100Nd@1Nd and to 32x61 nm for 100Nd@Y@1Nd.

In order to confirm that the nanoparticles synthesized in this work indeed demonstrate well-defined core-shell structures, the STEM-EDS elemental maps were recorded. For EDS mapping the core@shell@shell 100Nd@Y@1Nd sample was chosen as it has the most complicated structure and shows the most promising application properties. Here, we focused on Nd^{3+} and Y^{3+} distributions throughout nanoparticles by analyzing Nd L_α and Y L_α EDS lines in each pixel. The final distributions were overlaid and are presented in Figure S3a. While the morphology distribution is fairly good (Figure S2), the composition maps reveal some inhomogeneity of ion distribution within single nanoparticles depending on their orientation on the TEM grid. Nevertheless, Nd^{3+} rich core covered with Y^{3+} rich shell can be easily noticed. We also summed the point spectra over core and shell areas of an exemplary particle. These resultant sum spectra were normalized to Y L_α intensity and are shown in Figure S3b. The spectra confirm that the inner and outer regions, i.e. the core and the shell, are enriched in neodymium and yttrium, respectively. Such a procedure provides a validity check for EDS maps which usually involve the processing of noisy, low-intensity EDS spectra. Indeed, even though 80 keV energy was employed, the analyzed nanoparticles were sensitive to beam damage and required low-dose conditions (low beam current and short dwell time).

The core@shell@shell 100Nd@Y@1Nd nanoparticles were designed and synthesized to contain two shells that chemically differ by only 1% of neodymium. The maps in Figure 3a shows neodymium content up to the perimeter of nanoparticles instead of an abrupt cutoff. However, with only 1% Nd concentration and low-dose conditions used for the acquisition, we can only speculate that the EDS maps show two shells. Therefore, we shall conclude that the presented images provide only hints the 100Nd@Y@1Nd nanoparticles indeed display the desired architecture. More reliable confirmation is based on the spectroscopic results presented in main text, where we demonstrate that inner, inactive $NaYF_4$ shell separating $NaNdF_4$ core and outer $NaYF_4$:1%Nd shell results in the markedly enhanced luminescent quantum efficiency.

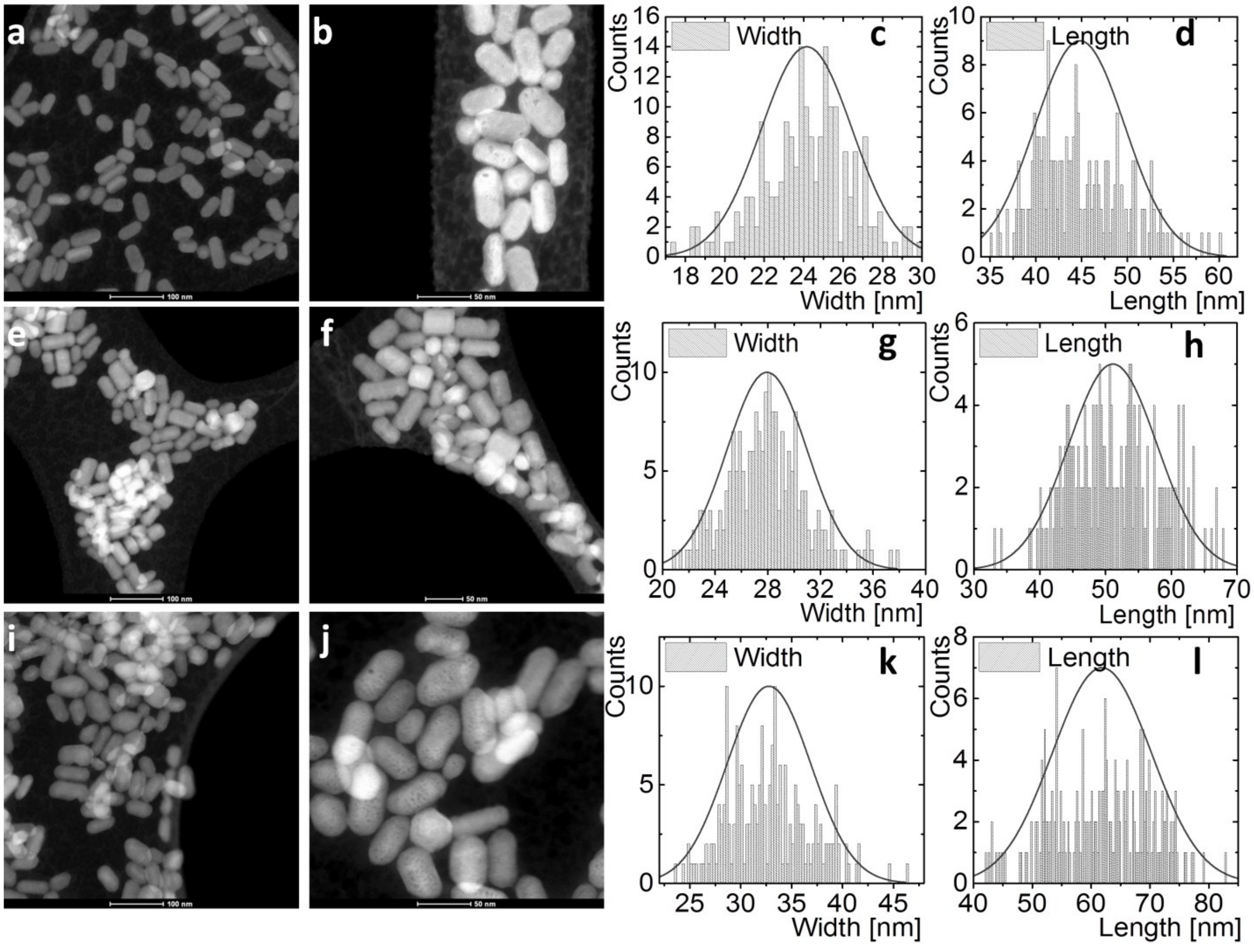

Figure S2. Representative STEM-HAADF images and size distribution histograms for core 100Nd (a-d), core@shell - 100Nd @ 1Nd (e-h) and core @shell @shell – 100Nd @ Y @ 1Nd (i-l) nanocrystals

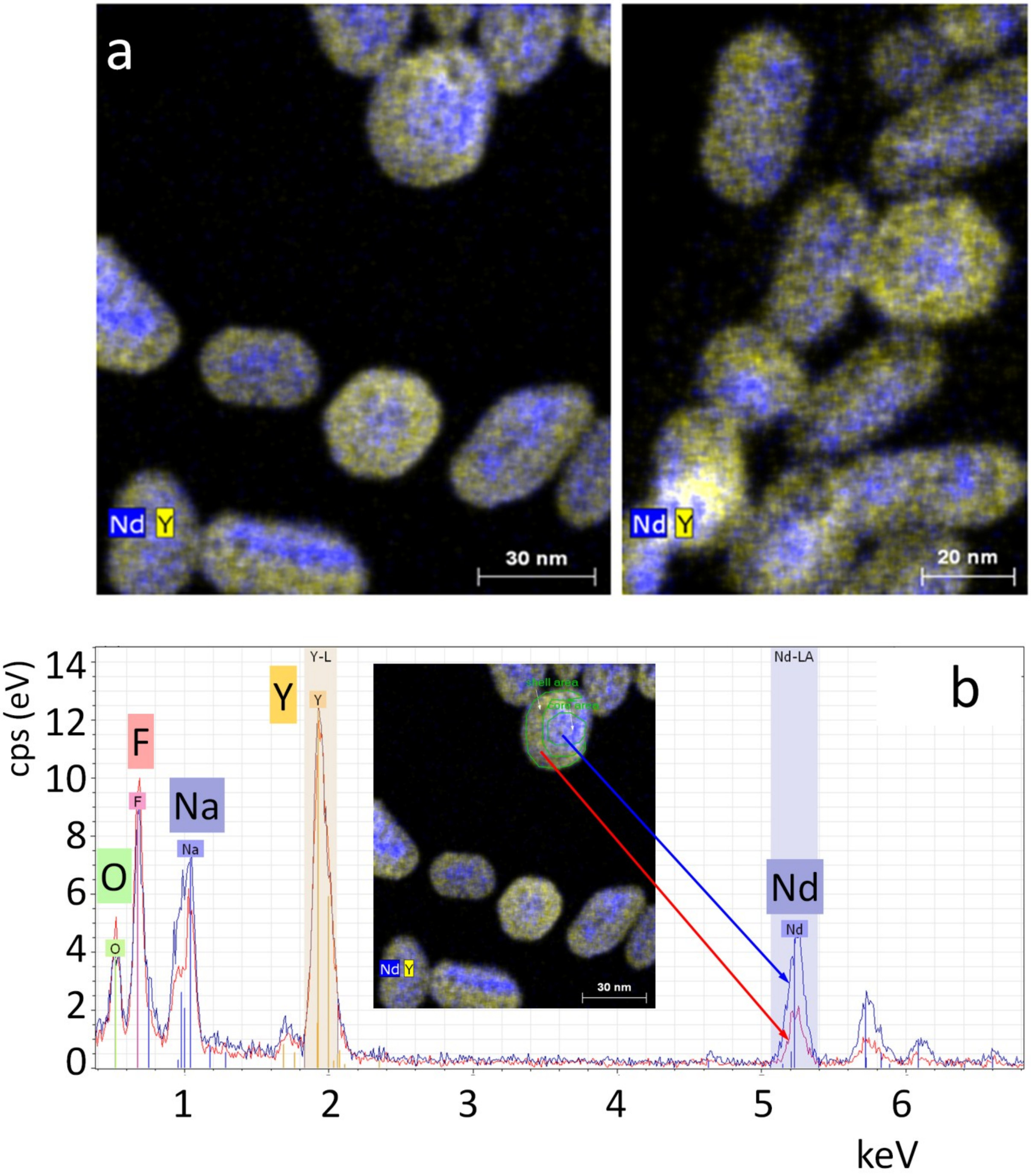

Figure S3. (a) Representative false-colour maps of chemical composition of 100Nd@ Y @1Nd nanoparticles showing distribution of Nd^{3+} (blue) and Y^{3+} (yellow) ions; (b) The synthesized and normalized (to Y L line) sum EDS spectra from inner and outer regions of the exemplary nanoparticle.

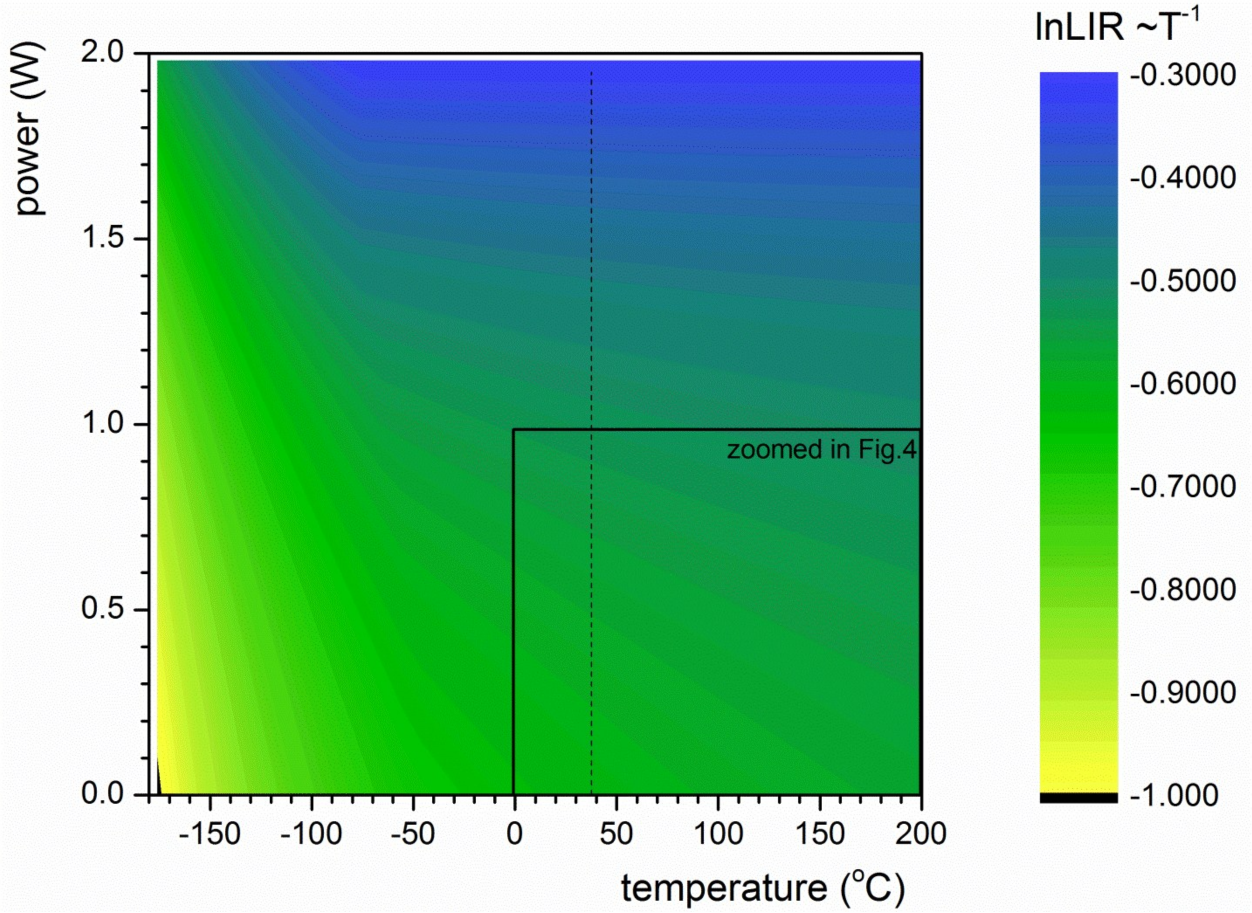

Figure S4. The extrapolated behavior of the optical nano-heater and nano-thermometer NPs. Ln(LIR), which is proportional to inverse of local temperature of the NP is presented versus the excitation intensity (Y axis) and macroscopic temperature (X axis). Dashed line represents physiological temperate. The rectangle is zoomed in Figure 5a.

Double beam experiment

While the use of NHNT nanoparticles for practical light induced hyperthermia is potentially beneficial, it may also bring some risks. The light beam, on its whole path from the surface of the skin down to subcutaneous layers, may induce heating and the beam is getting dimmer along the path due to scattering and absorption. Therefore, a risk of overheating becomes a serious issue. The solution can be the use to two (or more) sub-threshold laser beams, which independently are safe and become effective when they overlap. To verify such a possibility a proof-of-concept experiment was performed. The 100Nd @ Y @ 1Nd sample was drop casted on the glass slide and dried in air. The actual temperature maps were obtained with termovision camera from the thin sample layer fixed in a holder and illuminated superficially by the two activation laser beams of similar intensity (50mW@980nm). This approach was important because the bolometric cameras can only visualize the surface of the heated sample and not interior of bulk materials. The incidence angle of the two beams (Figure S5a red and orange arrows) differed in order to verify volumetric confinement of light induced heating. The negative control was made by using glass slide alone, without the sample material, which did not show the temperature increase (Figure S5).

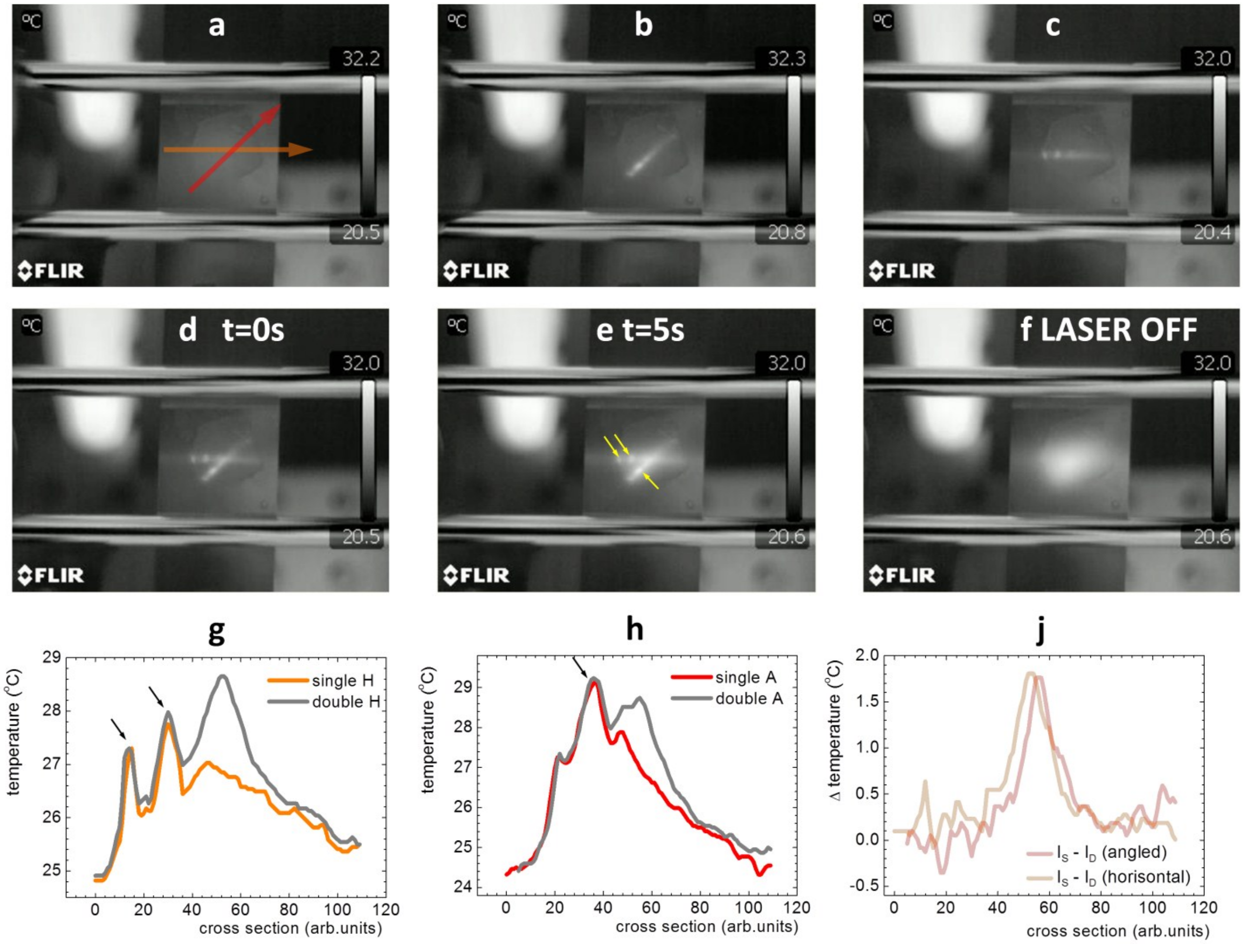

Figure S5. The temperature maps of the 100Nd@ Y @1Nd sample obtained with termovision camera under two laser beams of similar (50mW@980nm) intensity (red and orange arrows); (a) the situation before the experiment, the red and orange arrow indicate the direction and location of the two laser beams; (b) the 100Nd@ Y @1Nd sample illuminated with only angled beam (red); (c) the same sample illuminated with only horizontal beam (orange); (d) the sample illuminated with the two angled (red) and horizontal (orange) beams simultaneously, immediately after switching the two laser beams on; (e) the sample illuminated with the two angled (red) and horizontal (orange) beams simultaneously, after 5 seconds of illumination with the two laser beams on; (f) the temperature map immediately after switching the laser beams off; (g-h) the intensity profile line along the individual horizontal (orange-g) and angled (red-h) laser beams, the grey profiles arise from switching the second beam on; the difference between respective intensity profiles from (g) and (h).

One would expect the temperature rise resulting from the two overlapping beams will be twice higher as compared to a single beam (i.e. $T_{double} = 2\ T_{single}$). However, this was not the case and $T_{double} < 2\ T_{single}$. This deviation and the inhomogeneity of the intensity profiles (yellow arrows in Figure S5e and black arrows in Figure S5g,h) arise most probably from inhomogeneity of the sample, imperfections in beams overlap and the way the laser beams enter the sample. Similar observations were made with both termovision camera (Figure S5) and spectral measurements (LIR). The latter were performed with a spectrophotometer and optical fiber facing a small (0.5 mm diameter) sample area.

Despite some departures from expectations, in this proof of concept experiment by using two-beam hyperthermia (HT) the temperature increased by 2°C (Figure S5 j) in a confined volume immediately after switching the two lasers on. After prolonged exposure to laser light and owing to heat diffusion, the overheating region extends beyond the laser beams themselves and the photo induced HT is not confined to photo-illuminated area anymore.